Supporting Information

Amine-based solvents for exfoliating graphite to graphene outperform the dispersing capacity of *N*-methyl-pyrrolidone and surfactants

Zhenyu Sun, [a,b] Xing Huang,[c] Fang Liu,[d] Xiaoning Yang,*[d] Christoph Rösler,[e] Roland A. Fischer,[e] Martin Muhler[b] and Wolfgang Schuhmann[a]*

[a] *Analytical Chemistry - Center for Electrochemical Sciences (CES), Ruhr-Universität Bochum, D-44780 Bochum, Germany. E-mail: zhenyus@iccas.ac.cn*

[b] *Laboratory of Industrial Chemistry, Ruhr-Universität Bochum, D-44780 Bochum, Germany*

[c] *Fritz Haber Institute of the Max Planck Society, D-14195 Berlin, Germany*

[d] *College of Chemistry and Chemical Engineering, Nanjing University of Technology, 210009 Nanjing, the People's Republic of China*

[e] *Inorganic Chemistry, Ruhr-Universität Bochum, 44780 Bochum, Germany*

Experimental

Materials: All chemicals were of analytical grade and used as supplied. 3,3'-iminobis(*N*,*N*-dimethylpropylamine) (product number 348554), *N*-[3-(dimethylamino)propyl]methacrylamide (product number 409472), bis[2-(*N*,*N*-dimethylamino)ethyl] ether (product number 667609), 2-(*tert*-butylamino)ethyl methacrylate (product number 444332), 2-(dimethylamino)ethyl methacrylate (product number 234907), 2-[[(butylamino)carbonyl]oxy]ethyl acrylate (product number 496952), 2-(diethylamino)ethyl methacrylate (product number 408980), 3-(diethylamino)propylamine (product number 549975), 2-(butylamino)ethanol (product number 471496), *N*-methyl-2-pyrrolidinone (product number 328624), *N*,*N*-dimethylformamide (product number 227056), anionic surfactants sodium taurodeoxycholate (product number T0875) and sodium cholate (product number C1254), polyvinylpyrrolidone (product number 856568), and 2-methylimidazole (product number M50850) were purchased from Sigma-Aldrich. Graphite powder (product number 332461) was also acquired

from Sigma-Aldrich and used without further treatments. Zinc nitrate hexahydrate (product number 231-943-8) was purchased from J. T. Baker.

Liquid exfoliation of graphite to make graphene: Pristine layered graphite flakes were used as starting material for graphene exfoliation. Typically, graphene dispersions were prepared by adding graphite to 2.5 mL dispersant (5 mL vial) with the aid of ultrasonication (tip sonicator, Bandelin Sonoplus HD3100, 100 W, 20 kHz, 3 mm-diameter tip), a technique commonly used to accelerate exfoliation.[1] After 1 h of ultrasonication, samples were left to stand overnight to allow any unstable graphite aggregates to form and then centrifuged (Milipore-amicon MC-13). After centrifugation at 3000 rpm for 30 min, the top two-thirds of the dispersions were gently extracted by pipetting.

Pre-exfoliated graphite powder was formed by bath ultrasonication of graphite in isopropanol ($C_{G,I}$ = 10 mg mL^{-1}, t_{sonic} = 12 h) followed by vacuum evaporation of the supernatant of centrifuged dispersions (2000 rpm, 30 min).

Room-temperature synthesis of ZIF-8 nanocrystals or ZIF-8/FLG nanocomposites in MAEMA: Typically, 100 μL of $Zn(NO_3)_2 \cdot 6H_2O$ (54 mg mL^{-1}) in methanol solution was added into 5 mL of MAEMA or graphene dispersions in MAEMA, followed by addition of 100 μL of 2-methylimidazole (30 mg mL^{-1}) dissolved in methanol. The mixture was subjected to shaking by hand for 1 min and left for incubation at room temperature for around 15 h. Subsequently, the precipitates were collected by centrifugation and washed three times with methanol and then vacuum-dried at ambient conditions.

Characterization: The exfoliation level and quality of graphene dispersions were evaluated by multiple characterizations, including UV-Vis absorption spectroscopy, X-ray diffraction (XRD), X-ray photoelectron spectroscopy (XPS), thermogravimetric (TGA) measurement, scanning electron microscopy (SEM), transmission electron microscopy (TEM) and Raman spectroscopy. UV-Vis absorption was measured using a Varian Cary 60 spectrophotometer. XRD was performed with a D/MAX−RC diffractometer operated at 30 kV and 100 mA with Cu Kα radiation. XPS measurements

were carried out in an ultra-high vacuum (UHV) setup equipped with a monochromatic Al Kα X-ray source (hv = 1486.6 eV), operated at 14.5 kV and 35 mA. The base pressure in the measurement chamber was maintained at about 2×10^{-9} mbar. The resolution spectra were carried out in the fixed transmission mode with pass energy of 200 eV, resulting in an overall energy resolution of 0.25 eV. A flood gun was applied to compensate the charging effects. The binding energy scales were re-calibrated based on the C 1s peak of low-defect pure graphite at 284.6 eV. TGA analysis was conducted on a Netzsch STA 409 PC/PG instrument in an air atmosphere. SEM measurements were carried out using a field emission microscope (FEI Quanta 600 FEG) operated at 20 kV and equipped with an energy-dispersive X-ray spectrometer. TEM and high-resolution TEM images were recorded with a transmission electron microscope (Cs-corrected Titan) operated at 300 kV. TEM samples were prepared by pipetting a few milliliters of the dispersion onto holey carbon mesh grids (400 mesh). By carefully examining the edges of folded flakes one is able to count the number of fringes and thus the thickness of graphene layers. However, given the limited number of flakes counted and stacking of flakes, TEM counting unlikely gives reliable thickness distribution statistics. Raman spectra of graphene films and graphite powder were collected with a Horiba Jobin Yvon LabRam 2 confocal Raman microscope with a HeNe Laser excitation at 633 nm (1.96 eV) with a power of 3.5 mW. Deposited thin films were prepared by vacuum filtration onto porous nylon membranes (Whatman, 0.2 μm pore size, 47 mm membrane diameter) and dried at room temperature. We should point out that the filtered solvent could be recycled for further exfoliation use, significantly reducing the production cost. Measurements were taken with 5 s of exposure time using a long working distance objective of 50-fold magnification and aperture 0.5 yielding a beam diameter of ~600 nm in the focus. The peak maximum intensity ratio I_D/I_G was obtained by taking the peak intensities following baseline corrections to remove residual fluorescence. Conductivity measurements were performed using a custom-made high-throughput test stand equipped with a four-point probe head. Five measurements were conducted for each sample and the conductivity values were averaged. Measurement current was 1 mA pulsed DC in

all cases. The sample for conductivity measurement was prepared by vacuum filtering the dispersions in MAEMA ($C_{G,I}$=10 mg mL^{-1}, t_{sonic}=1 h, centrifugation: 3000 rpm, 30 min) onto porous membrane. Taking into account the fact that the solvent remaining has adverse effects on the film conductivity, the sample was subjected to vacuum drying at 60 ºC for 48 h to remove most bulk and adsorbed solvent molecules. The thickness of the film sample was determined by SEM. CO_2 adsorption (195 K) of FLG and ZIF-8/FLG composites was measured using BELSORP-max analyzer.

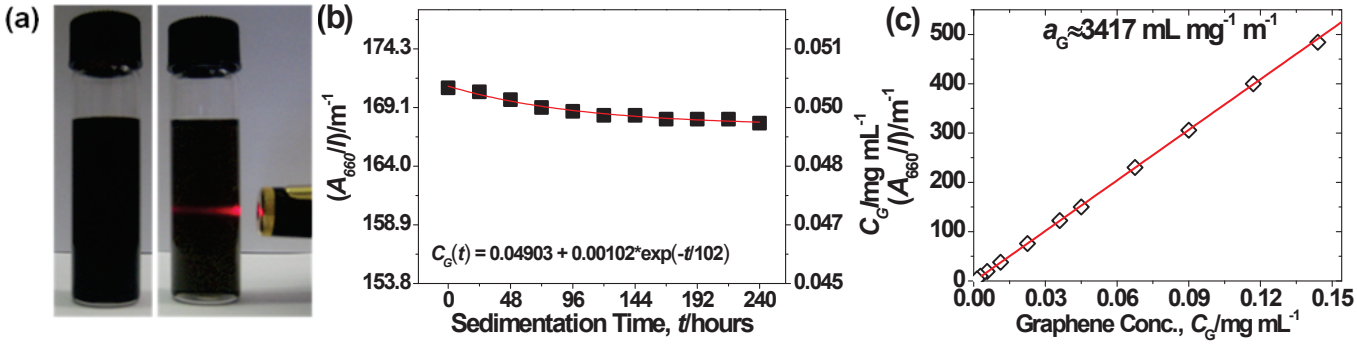

Fig. S1 (a) Photograph of graphene dispersions in BAEMA. Left to right: centrifuged for 30 min at 3000 rpm, diluted by a factor of 10 after centrifugation. (b) The absorbance per unit-cell-length at 660 nm (A_{660}/l) versus sedimentation time (t) for the BAEMA dispersion (graphene concentration C_G=0.05 mg mL^{-1}). An exponential decay was observed which can be well approximated by $c(t) = c_0 + Ae^{-t}/\tau$, in which c_0 is the concentration of the stable phase, τ corresponds to the sedimentation time constant. Fitting the data gave c_0/c_T≈0.98 (c_T is the inital dispersion concentration) and τ=102 h. (c) A_{660}/l as a function of C_G in MAEMA. The concentration of the original dispersion for dilution was determined by TGA analysis together with the knowledge of the mass of graphitic material+MAEMA remaining after evaporation of the solvent for known volumes of dispersions. A straight line fit through the points gave the absorption coefficient at 660 nm of α=3417 mL mg^{-1} m^{-1}. The initial graphite concentration ($C_{G,I}$) in (a)-(c) is 10 mg mL^{-1}.

DMAPMA, BAEMA and MAEMA compare more favourably than the most common graphene solvent, NMP, from the viewpoint of cost and hazard associated with the solvent. NMP costs €114.5

per liter (Aldrich, anhydrous grade). By comparison, DMAPMA costs €118 per liter, MAEMA is slightly cheaper (€99.2 per liter, Aldrich). Given the higher dispersion concentration relative to NMP, BAEMA (€253 per liter, Aldrich) is not much prohibitive. In terms of toxicological considerations, NMP is classified as dangerous which may damage the unborn child whereas DMAPMA, BAEMA and MAEMA are irritants to eyes and skin. DMAPMA offers maximum dispersibility coupled with much milder toxicological concerns than other reported graphene solvents (e.g., DMF, which has been thought to cause birth defects and cancer in humans).

Table S1 A_{660}/l of graphene dispersions in the nine amine solvents as well as in NMP, DMF and the aqueous solutions of surfactants STC, SC and the polymer PVP ($C_{G,I}$=10 mg mL^{-1}).

Chemicals	A_{660}/l (m^{-1})	Standard Error
3,3'-iminobis(*N*,*N*-dimethylpropylamine)	781.5	59.3
N-[3-(dimethylamino)propyl]methacrylamide	626.4	138.8
2-(*tert*-butylamino)ethyl methacrylate	576.1	10.3
2-(dimethylamino)ethyl methacrylate	504.5	29.8
2-[[(butylamino)carbonyl]oxy]ethyl acrylate	208.4	0.92
2-(diethylamino)ethyl methacrylate	156.2	2.6
bis[2-(*N*,*N*-dimethylamino)ethyl] ether	105.1	12.4
3-(diethylamino)propyl amine	77.6	0.1
2-(butylamino)ethanol	42.0	0.74
N-methylpyrrolidone (NMP)	474.3	134.0
dimethylformamide (DMF)	62.3	18.1
sodium taurodeoxycholate (STC)	445.6	32.9
sodium cholate (SC)	330.0	66.8
Polyvinylpyrrolidone(PVP)	234.9	67.6

During ultrasonication, shear forces and cavitation act on the bulk graphite and can overcome the interlayer van der Waals attractions (61 meV/C atom), thereby leading to exfoliation. The strong solvent-graphene interactions can minimize the area of the surfaces in contact, thus stabilizing graphene sheets against aggregation. To minimize the defects and/or damage induced during cavitation, short periods of ultrasonication (1 h) was applied here. For optimization of the exfoliation process, we first investigated the dispersibility of graphene in MAEMA versus ultrasonic intensity, which was maximised at 6 W cm^{-2} (Fig. S2a). This may suggest that too-high a sonication power may have destroyed the aggregated structures of the solvent that was adsorbed onto graphene, consequently leading to the degradation of its exfoliation. We also considered the effect of ultrasonic bath temperature (T_{sonic}) on the dispersion (inset in Fig. S2a). We found that C_G increases along with T_{sonic} in the range 0-10 ºC, followed by a decrease at T_{sonic}>10 ºC. A possible reason for this is that higher T promotes better adsorption of MAEMA onto graphene and thus more dispersed objects. At higher T_{sonic}>10 ºC, the impact of temperature on cavitation may play a key role; that is, it was more difficult for cavitation to collapse given an increase in temperature, thus resulting in reduction of output power, and consequently lower levels of graphene exfoliation. In light of these results, we chose to prepare subsequent graphene dispersions at T_{sonic}=10 ºC.

C_G was measured as a function of $C_{G,I}$ (Fig. S2b). It was observed that C_G increases steadily with $C_{G,I}$, reaching a peak value at $C_{G,I}$=10 mg mL^{-1}. It is likely that more starting graphite provides more adsorption sites for stabilizer molecules. However, amounts of graphite that were too high may prevent the efficiency of ultrasonication and exfoliation, thereby leading to a decrease in C_G at $C_{G,I}$ > 10 mg mL^{-1}. Recyling the sediment allows an increase of the yield of graphene further.

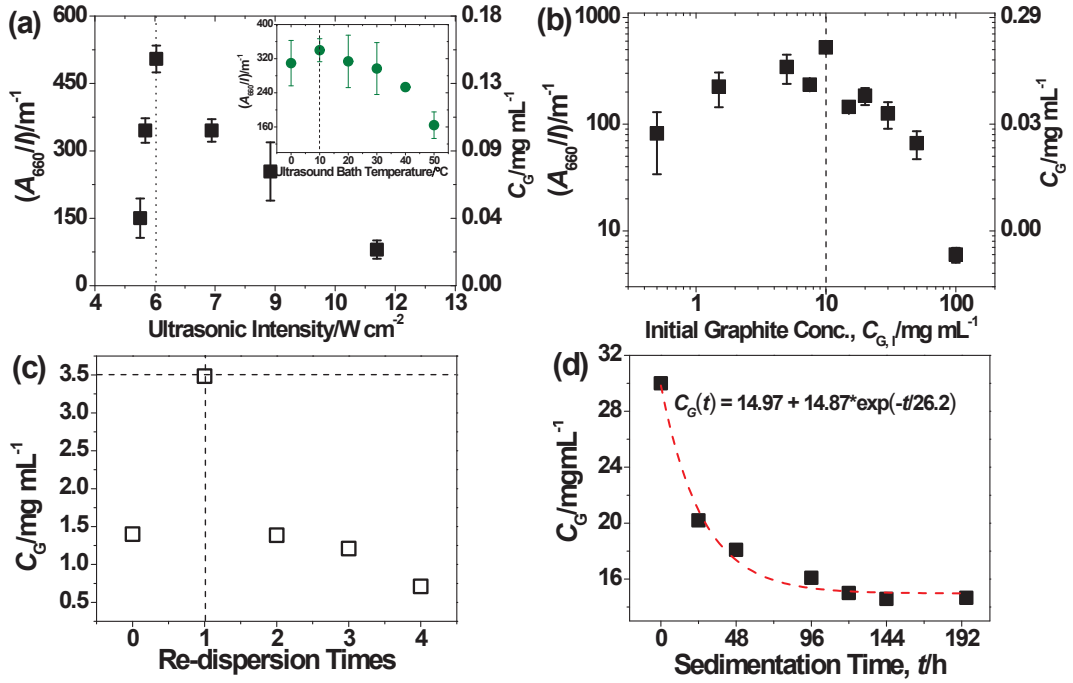

Fig. S2 (a) A_{660}/l as a function of ultrasonic intensity. Inset: A_{660}/l versus ultrasound bath T at an ultrasonic intensity of 6 W cm^{-2} ($C_{G,I}$=10 mg mL^{-1}). (b) A_{660}/l as a function of initial graphite concentration. (c) Dispersed concentration at different re-dispersion times for the sediments (starting material: pre-exfoliated graphite powder in isopropanol, $C_{G,I}$=10 mg mL^{-1}, t_{sonic}=1 h, centrifugation: 3000 rpm, 30 min) redispersed via bath sonication (15 min) using BAEMA. (d). Stability profile of the system resulting from the re-dispersion of filtered few-layer graphene powder. It exhibits an exponential decay that can be satisfactorily approximated by $c(t)$ = 14.97 + 14.87e$^{-t/26.2}$. Note that the dispersion concentration was still quite high (≈15 mg mL^{-1}) after 8 days. This will facilitate its further processing and applications.

Models and simulation method

In this simulation, the non-bonded interactions were represented by a sum of the Coulomb and Lennard-Jones terms as Equation (1),

$$E_{ab} = \sum_i^a \sum_j^b \left[\frac{q_i q_j e^2}{r_{ij}} + 4\epsilon \left(\frac{\sigma_{ij}^{12}}{r_{ij}^{12}} + \frac{\sigma_{ij}^{6}}{r_{ij}^{6}} \right) \right] \qquad (1)$$

in which E_{ab} is the interaction energy between centers *a* and *b*. The intramolecular interaction includes the bond stretching and bond bending. The MAEMA molecule was simulated using the united-atom OPLS force field,[2-9] in which CH_2 and CH_3 group were represented by imaginary atom. Atomic charges were calculated according to the QEq method. All the force field parameters were listed in Table S2. The carbon atoms in graphene were modelled as uncharged Lennard–Jones (LJ) particles.[10] The van der Waals interactions of different atoms were calculated by the geometric averaging rule: $\varepsilon_{ij} = \sqrt{\varepsilon_i \varepsilon_j}$, $\sigma_{ij} = \sqrt{\sigma_i \sigma_j}$ .To check the reliability of the force field, we have simulated the bulk phase of MAEMA and calculated the bulk density. The value of simulation is 0.966 g/cm^3, which is close to the experimental data of 0.933 g/cm^3.[11]

All MD simulations were conducted by using the Lammps code (http://lammps.sandia.gov/).[12] NPT ensemble was used with the Nose–Hoover thermostat and barostat. The particle-mesh Ewald (PME) method was used to calculate the electrostatic interactions. Periodic boundary condition was applied in all three directions. The graphene sheets were simulated as a rigid body. A standard velocity-Verlet integrator was used for molecular dynamics simulations with time step equal to 1 fs. In the interfacial structure simulation, the graphene sheet was placed at z=0 and spanned the x-y plane. Each simulation was run for 10 ns to achieve equilibrium in NPT ensemble with system pressure of 1 atm and temperature of 298.15 K. As the graphene sheet limited the size of the simulation box in x-y plane, the Nose–Hoover barostat was only applied along the z direction.

We calculated the change of free energy (potential of mean force, PMF) for the exfoliation/aggregation process by steered molecular dynamics (SMD) simulation.[13] In the exfoliation process, the initial distance between two graphene sheets was set to be 3.4 Å, and the right graphene was pulled away from the left sheet. For the aggregation, the initial distance was set to be 18.4 Å between two graphene sheets. A constant-velocity SMD simulation was performed with a velocity of 0.000005 Å/fs and a spring constant of 20 kal/mol/Å^2.

Table S2 Force field parameters for MAEMA.

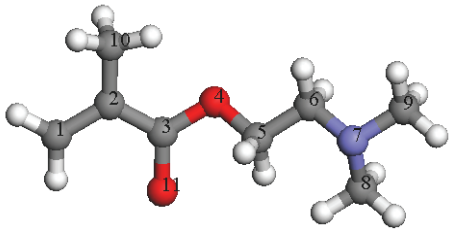

LJ parameters and partial charges for MAEMA

Atom number	Atom and atom group	q , e	ε , kal/mol	σ , Å
1	CH2=	0.035	0.153	3.761
2	C	0.022	0.076	3.550
3	C	0.548	0.105	3.750
4	O	-0.583	0.170	3.000
5	CH2	0.33	0.091	3.950
6	CH2	0.209	0.091	3.820
7	N	-0.369	0.170	3.250
8	CH3	0.13	0.190	3.660
9	CH3	0.135	0.190	3.660
10	CH3	0.042	0.195	3.750
11	O	-0.499	0.210	2.960

Bond Stretching Parameters

Bonds	Atom number	k_b , kal/mol	r_0, Å
1	1-2	549.0	1.350
2	2-3	410.0	1.444
3	3-4	374.3	1.330
4	4-5	369.7	1.430
5	5-6	309.2	1.530
6	6-7	258.5	1.490
7	7-8	258.5	1.500
8	7-9	258.5	1.500
9	2-10	317.0	1.510
10	3-11	684.5	1.220

Angle Bending Parameters

Angles	Atom number	k_θ, kal/mol/rad^2	θ_0
1	1-2-3	85.0	120.7
2	2-3-4	73.7	114
3	2-3-11	59.9	124
4	3-4-5	73.7	109.47
5	4-5-6	87.0	109.47
6	5-6-7	80.0	109.5
7	6-7-8	50.0	118.0
8	6-7-9	50.0	118.0
9	1-2-10	85.0	119.7
10	3-2-10	85.0	119.7
11	4-3-11	105.1	120
12	8-7-9	50.0	118.0

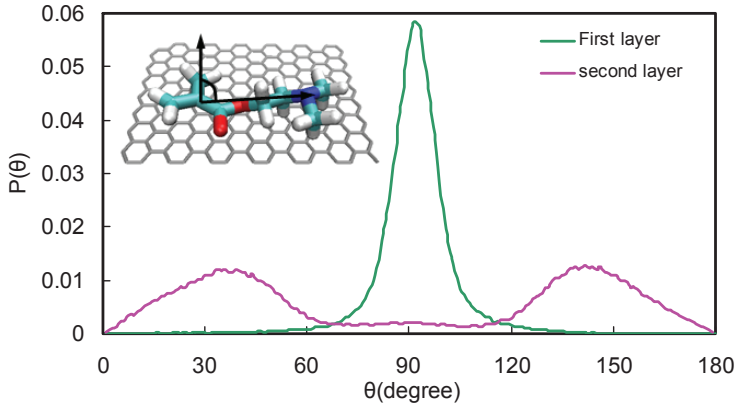

Fig. S3 The orientation distributions *P(θ)* in the isolated solvent layer with the first layer (from 3.6 Å to 5.2 Å in the interfacial density profile) and the second layer (from 5.2 Å to 7.8 Å). The inset is the definition of the orientation angle. The orientation of the first isolated layer present major peak at 90°, which illustrates most of MAEMA molecules paralleling to the surface of graphene. The orientation of the second isolated layer present two major peak at 40° and 140° as the MAEMA molecules inclining to the graphene surface.

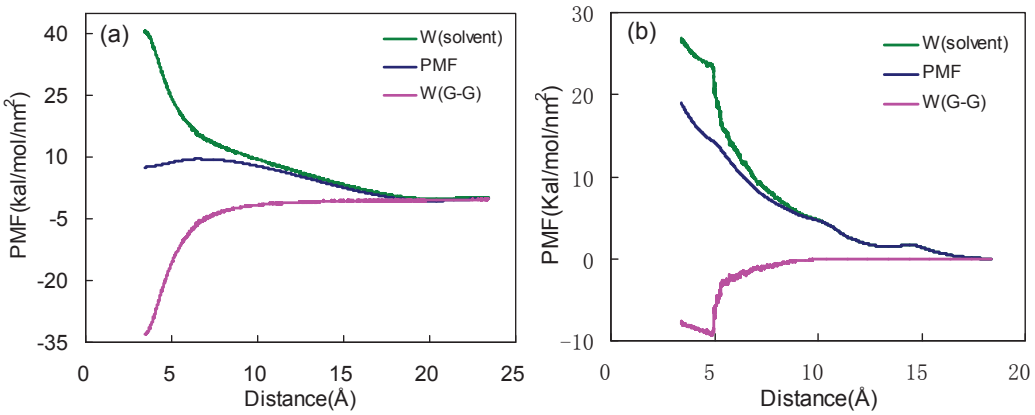

Fig. S4 The PMF and the decomposition as a function of graphene sheet separation distance. (a) the exfoliation process (b) the aggregation process. W (solvent) represents the solvent contribution to the free energy change; and W (G-G) is the contribution from the interaction between graphenes. From the exfoliation process (Fig. S4a), the direct interaction of graphene layers hinders the exfoliating dispersion of grapheme sheets, whereas the solvent-induced interaction can significantly improve the exfoliation of graphene sheets. In the aggregation process (Fig. S4b), the solvent-induced interaction

had a repulsive action on the aggregation of graphene sheets. For the separation distance near 5 Å, the abnormally changed free-energy might come from the slanting graphene during the aggregating process.

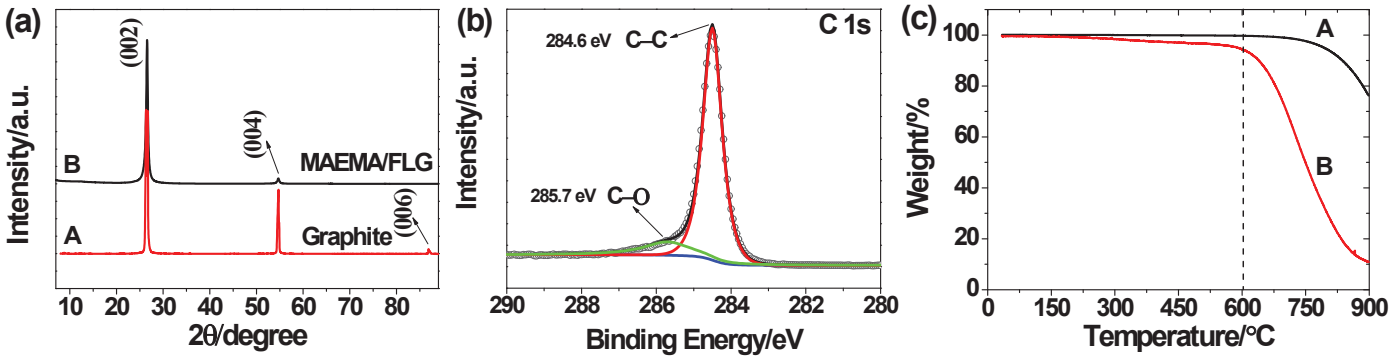

Fig. S5 (a) XRD pattern of the initial graphite (trace A), and the sample (trace B) resulting from the MAEMA/FLG dispersions after removal of the solvent by filtration and dried at room T. The diffraction peaks at ~26.8 and ~54.8º in both traces are attributed to the (002) and (004) reflections of the hexagonal graphite structure, respectively.[14] The two peaks in trace B appear at the same position as those in trace A, which suggests that the graphite lattice was retained after exfoliation. (b) C 1s XPS spectrum for a filtered graphene film. The C 1s region is dominated by a peak at around 284.5 eV, which corresponds to sp^2 graphitic carbon. Deconvolution of the spectrum manifested an additional small peak at 285.7 eV, which is assigned to C-O. (c) TG thermograms for graphite (trace A), and filtered MAEMA/FLG (trace B), obtained with a ramp rate of 10 K min^{-1} in air. A small weight loss <6 wt% occurred prior to 600 ºC for the graphene sample, akin to the original graphite. This stands contrast to the loss of acidic residues and functional groups between 180 and 220 °C for graphene oxide.[15]

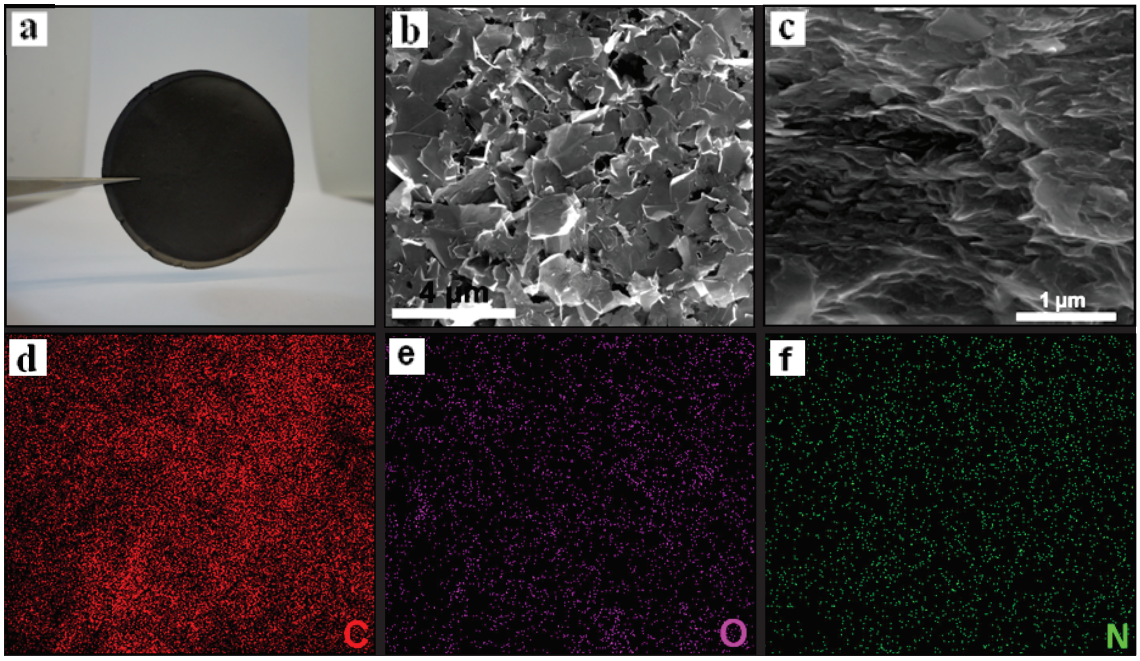

Fig. S6 (a) Photograph of a film formed by vacuum filtration of the graphene dispersions in MAEMA. SEM images of (b) the surface and (c) edge of the film. Energy-dispersive X-ray (EDX) maps of the region shown in (b): (d) C, (e) O, and (f) N. In addition to many small flakes of several hundred nanometers due to sonication-induced cutting, large sheets with dimensions of up to 5 µm in length were detected. The edge of the film consists of interconnected graphene nanosheets showing a well-defined layered morphology. The presence of O and N shown in the EDX pattern illustrates the adsorption of the solvent on the flake enabling the stabilization of graphene nanosheets.

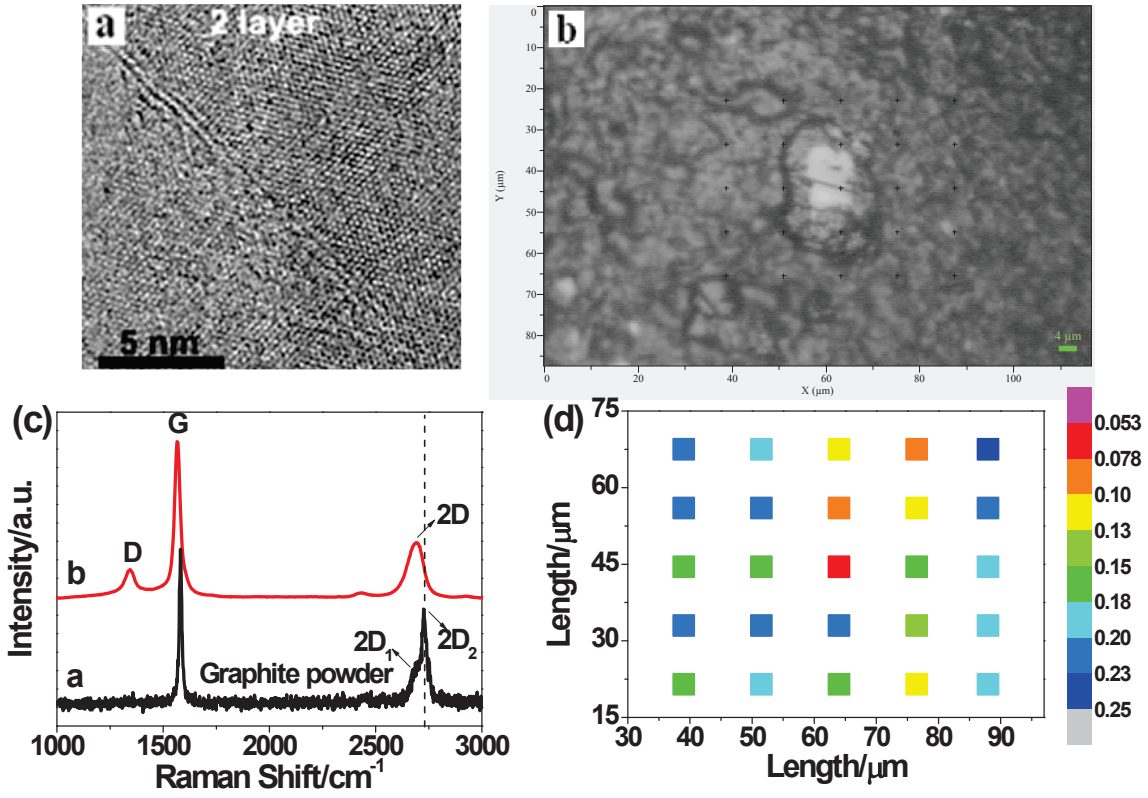

Fig. S7 (a) HRTEM image of a bilayer structure. Small variations of incidence angle in the surface resulted in pronounced electron contrast for few-layer graphene. (b) Optical microscopic image of the film sample formed by filtration from dispersions of MAEMA/FLG ($C_{G,I}$=10 mg mL^{-1}, t_{sonic}=1 h, centrifugation: 3000 rpm, 30 min). (c) Raman spectra (633 nm excitation) of the starting graphite (trace a) and the filtered film (trace b). The spectra were normalized based on the G mode peak intensity. The Raman spectrum of the thin film shows an intense G band at about 1564 cm^{-1}, a second-order two-phonon mode 2D (also called G') band at about 2687 cm^{-1}, and a disorder-related D peak at about 1344 cm^{-1} (trace b). The G band corresponds to the E_{2g} phonon at the Brillouin zone center, whereas the D band is associated with longitudinal optic (LO) phonons.[16] The 2D line can be well fitted with a single symmetrical Lorentzian peak, which is qualitatively in agreement with the Raman spectrum of few-layer graphene flakes that are positioned one on top of the other in a random orientation.[1,14] This observation is in contrast to the doublet 2D shape for graphite, which consists of two components, $2D_1$ and $2D_2$, indicative of an unperturbed ABAB stacking sequence along the c

direction of the bulk material. A shift of approximately 37 cm^{-1} to lower wavenumbers occurs for the 2D band of the film sample relative to graphite. (d) Two-dimensional Raman map of the regions for the film as shown in (b). The color gradient bar to the right of the map represents the D-to-G peak intensity ratio.

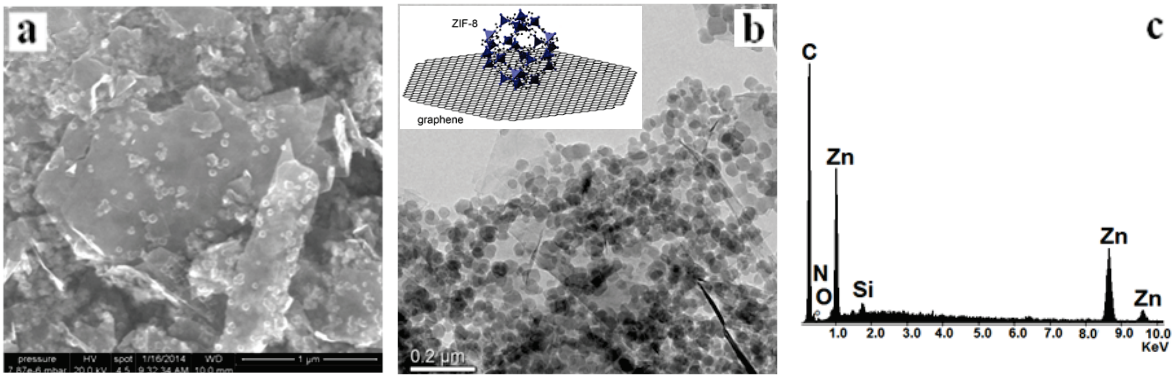

Fig. S8 (a) SEM and (b) TEM observations of ZIF-8/FLG. It is clearly seen that ZIF-8 NPs were well-dispersed on the surface of few-layer graphene. No free-standing particles detached from graphene were found. We speculate that the amine solvent molecules adsorbed on FLG may promote the formation of ZIF-8 nanocrystals and also their preferable deposition on the graphene surface. Inset: Schematic of the structure of ZIF-8/FLG. (c) EDX pattern. The presence of Zn and N suggests the formation of ZIF-8 in the sample. The element Si may originate from the original graphite.

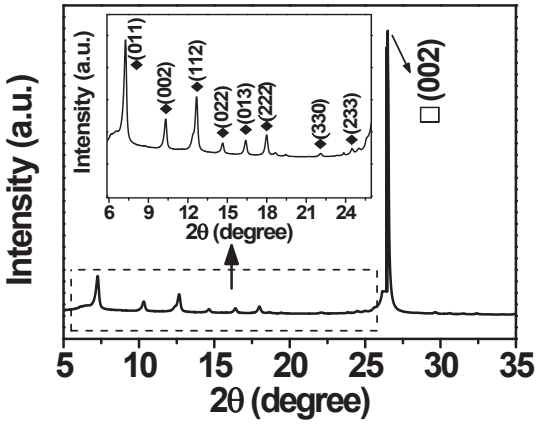

Fig. S9 X-ray diffraction spectroscopy (XRD) pattern of ZIF-8/FLG. The inset shows the enlarged regime enclosed by the dashed line. The formation of ZIF-8 was confirmed by XRD with diffraction

peaks in the range 5-25º matching well with those reported in literature.[17] The strong diffraction peak around 26.5º arises from the (002) reflection of the hexagonal graphite structure in the composite.

1 Z. Y. Sun, J. Masa, Z. M. Liu, W. Schuhmann and M. Muhler, *Chem.-Eur. J.,* 2012, **18**, 6972-6978.

2 F. J. A. L.Cruz and E. A. Mueller, *Adsorption,* 2009, **15**, 1-12.

3 W. L. Jorgensen, D. S. Maxwell and J. TiradoRives, *J. Am. Chem. Soc.,* 1996, **118**, 11225-11236.

4 W. L. Jorgensen, J. M .Briggs and M. L. Contreras, *J. Phys. Chem.,* 1990, **94**, 1683-1686.

5 Z. A. Makrodimitri, D. J. M. Unruh and I. G. Economou, *J. Phys. Chem. B,* 2011, **115,** 1429-1439.

6 Z. P. Liu, T. Chen, A. Bell and B. Smit, *J. Phys. Chem. B,* 2010, **114,** 4572-4582.

7 S. J. Weiner, P. A. Kollman, D. T. Nguyen and D. A. Case, *J. Comput. Chem.,* 1986, **7**, 230-252.

8 K. J. Lin and J. K. Maranas, *Macromolecules,* 2012, **45**, 6230-6240.

9 S. J. Weiner, P. A. Kollman, D. A. Case, U. C. Singh, C. Ghio, G. Alagona, S. Profeta, Jr. and P. Weiner, *J. Am. Chem. Soc.,* 1984, **106**, 765-784.

10 C. J. Shih, S. C. Lin, M. S. Strano and D. Blankschtein, *J. Am. Chem. Soc.,* 2010, **132**, 14638-14648.

11 D. Solpan, M. Sen, Z. Kolge and O. Guven, *Radiat. Phys. Chem.*, 2008, **77**, 428-433.

12 S. Plimpton, *J. Comput. Phys.*, 1995, **117**, 1-19.

13 S. Park, F. K. Araghi, E. Tajkhorshid and K. Schulten, *J. Chem. Phys.,* 2003, **119**, 3559-3566.

14 Z. Y. Sun, N. N. Dong, K. P. Wang, D. König, T. C. Nagaiah, M. D. Sánchez, A. Ludwig, X. Cheng, W. Schuhmann, J. Wang and M. Muhler, *Carbon,* 2013, **62**, 182-192.

15 L. M. Viculis, J. J. Mack, O. M. Mayer, T. Hahn and R. B. Kaner, *J. Mater. Chem.,* 2005, **15**, 974-978.

16 A. C. Ferrari, J. C. Meyer, V. Scardaci, C. Casiraghi, M. Lazzeri, F. Mauri, S. Piscanec, D. Jiang, K. S. Novoselov, S. Roth and A. K. Geim, *Phys. Rev. Lett.,* 2006, **97**, 187401.

17 K. S. Park, Z. Ni, A. P. Cote, J. Y. Choi, R. D. Huang, F. J. Uribe-Romo, H. K. Chae, M. O'Keeffe and O. M. Yaghi, *Proc. Natl. Acad. Sci. U. S. A.,* 2006, **103**, 10186-10191.